

http://pubs.acs.org/journal/aelccp

# Amplifying Hole Extraction Characteristics of PEDOT:PSS via Post-treatment with Aromatic Diammonium Acetates for Tin Perovskite Solar Cells

Donghoon Song, Hao Li, Yuanze Xu, and Qiuming Yu\*



Cite This: ACS Energy Lett. 2023, 8, 3280-3287



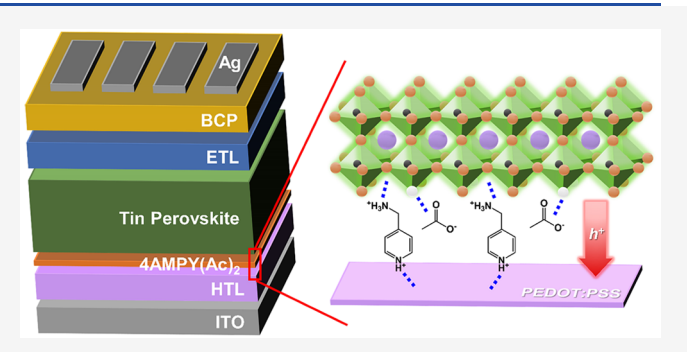
**ACCESS** I

III Metrics & More

Article Recommendations

S Supporting Information

ABSTRACT: We modify the PEDOT:PSS hole transport layer (HTL), commonly adopted for high-performance tin perovskite solar cells (TPSCs), via post-treatment of its surface using aromatic diammonium acetate salts dissolved in a highly volatile but interactive solvent. The solvent partly etches excessive insulating PSS while enabling tight anchoring of the salts to the PEDOT:PSS HTL. The salts improve not only the PEDOT:PSS/perovskite interface but also the top surface of tin perovskite thin films, leading to reduced interface defects, larger built-in potentials, and suppressed perovskite pinhole defects. In addition, the salts transform the PEDOT structure from benzoid to quinoid and depopulate excessive hole charge



carriers to promote hole extraction. Consequently, TPSCs attain a high efficiency of 12.1% under standard 1 sun light illumination and impressive stability without encapsulation for  $\sim$ 2800 h under an  $N_2$  atmosphere. We developed a straightforward but impactful method to modify PEDOT:PSS for broader applications.

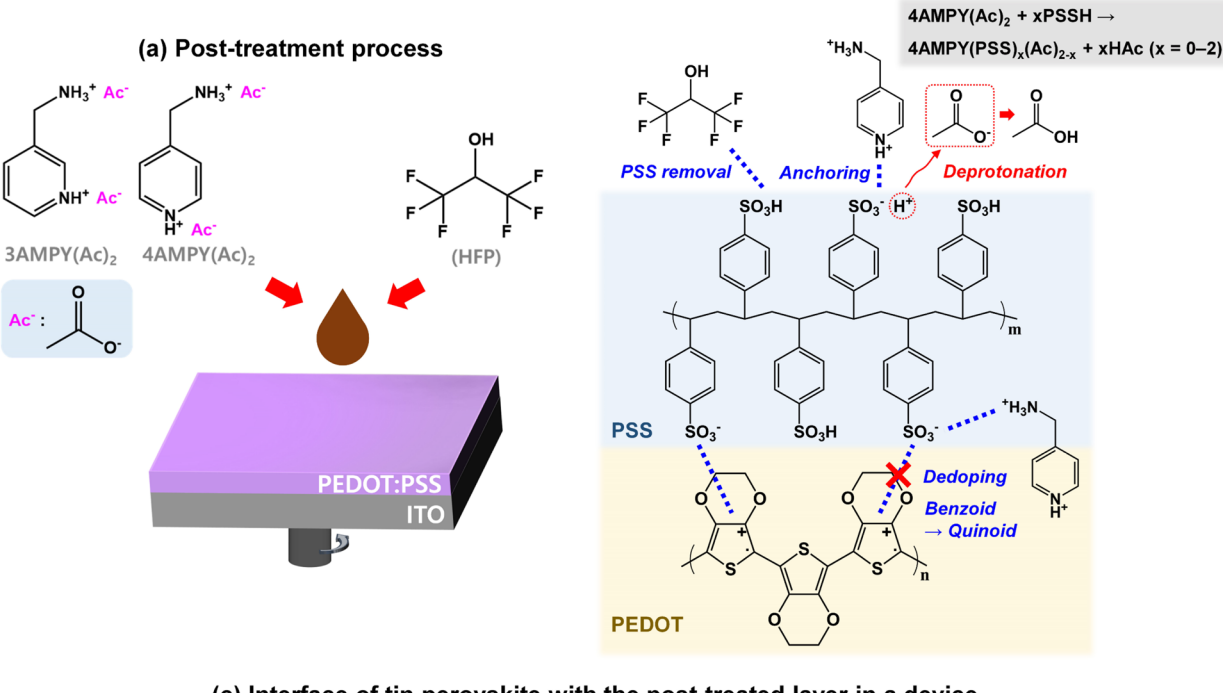
in perovskite solar cells (TPSCs) stand at the forefront as toxicity-lean technology, featuring compelling properties, including, for example, large light absorption coefficient, small exciton binding energy, ideal bandgap, slow hot-carrier cooling, and high charge carrier mobility. Especially, tin perovskites are adjustable to a bandgap of ~1.34 eV, which is optimal for single-junction solar cells according to the Shockley-Queisser limit.<sup>8</sup> Beyond merely a toxicity issue, such superb properties drive TPSCs to an efficiency of power conversion (PCE) close to 15%. To close the gap with that ( $\sim$ 26%) of lead counterparts, 11 tailoring tin perovskites to mitigate fast crystallization and Sn(II) oxidation and designing their interfaces to attain efficient and stable charge collection have proceeded. 9,10,12-20 Irrespective of what types of tactics are attempted, present-day TPSCs feature poly(3,4-ethylenedioxythiophene) polystyrenesulfonate (PEDOT:PSS) as a hole transport layer (HTL) due to the high performance and reproducibility in an inverted planar architecture. 9,10,13-19 The PEDOT:PSS benefits from the demanding properties for TPSCs, including a suitable work function (WF: ~5.0-5.2 eV), decent conductivity, and dopant-free nature. 21,22 However, it is desired to modify the PEDOT:PSS thin films to be better suited to TPSCs.

Among various HTLs, PEDOT:PSS suffers from high recombination velocity at the interface with perovskite, and it becomes more problematic with the decrease of perovskite film thickness (cf. film thickness: ~200 nm for tin perovskites vs ~500 nm or greater for lead perovskites).<sup>23</sup> Additionally, PSS is enriched at the surface, making it electrically insulating and hygroscopic.<sup>21,24</sup> Particularly because of the hygroscopic nature, residual water may be unavoidable upon ambient air annealing according to thermal analysis,<sup>25</sup> and it is likely during processing and storage even in a glovebox.<sup>21</sup> The permeation of ions across the PEDOT:PSS interface (i.e., electrochemical doping) to destabilize perovskite crystals could also occur.<sup>1,21</sup> On the other hand, it is generally accepted that defects in perovskites are more abundant at the interfaces of charge transport layers and perovskite films than in perovskite bulk,

Received: March 17, 2023 Accepted: July 6, 2023



# (b) Post-treatment mechanism



# Cc) Interface of tin perovskite with the post-treated layer in a device Defects-less tin perovskite Tin Halide PCBM or ICBA Tin Perovskite 3AMPY(Ac)<sub>2</sub> or 4AMPY(Ac)<sub>3</sub> PEDOT:PSS

Figure 1. Schematic illustrations of (a) process and (b) mechanism of post-treatment onto the PEDOT:PSS HTL whose interface in a device is described in panel c. In panels b and c, only  $4AMPY(Ac)_2$  is described for simplicity.

which can act as traps for nonradiative recombination.<sup>26</sup> We posit that tin perovskites coming into contact with PEDOT:PSS could not be free of this issue. Tailoring the interface toward an efficient and stable extraction of hole charge carriers remains a grand but necessary challenge in this regard.

We tackle this challenge via post-treatment of PEDOT:PSS using aromatic diammonium acetate salts dissolved in a highly volatile but interactive solvent. The experimental scheme of post-treatment is described in Figure 1a. We synthesized the salts of 3-(aminomethyl)pyridinium acetate and 4-(aminomethyl)pyridinium acetate, abbreviated hereafter as 3AMPY(Ac)<sub>2</sub> and 4AMPY(Ac)<sub>2</sub>, respectively. The synthesis details are given in the Supporting Information, and the chemical structures are displayed in Figure 1a. To dissolve 3AMPY(Ac)<sub>2</sub> and 4AMPY(Ac)<sub>2</sub>, we selected 1,1,1,2,2,2-hexafluoro-2-propanol (HFP) as a solvent; the solution concentration was optimized to be 0.5 mM as tested in the range of 0–5 mM (Figure S1 and Table S1). HFP has a similar

dielectric constant as 2-propanol and is able to dissolve a large family of organic salts, including 3AMPY(Ac)<sub>2</sub> and 4AMPY-(Ac)<sub>2</sub>. HFP is a fluorinated solvent that forms strong hydrogen bonds with the functional group -SO<sub>3</sub>H in PSS as depicted in Figure 1b. This interaction can result in a slight removal of PSS along with the evaporation of HFP. It also helps the insertion of 3AMPY(Ac), and 4AMPY(Ac), in the top-enriched PSS for further interaction with the PEDOT:PSS layer. On the other hand, HFP undergoes quick evaporation even at room temperature due to the high volatility, likely modifying the surface rather than the bulk. The atomic force microscopic (AFM) images show non-noticeable changes to the surface morphologies and roughness of the post-treated PEDOT:PSS films compared to the pristine one (Figure S2). We highlight that our post-treatment is in striking contrast with blending PEDOT:PSS with additives as the bulk properties of PEDOT:PSS are varied in those treatments.<sup>21</sup>

We discuss the merits of the molecular structures of 3AMPY(Ac)<sub>2</sub> and 4AMPY(Ac)<sub>2</sub> for the post-treatment of

ACS Energy Letters http://pubs.acs.org/journal/aelccp Letter

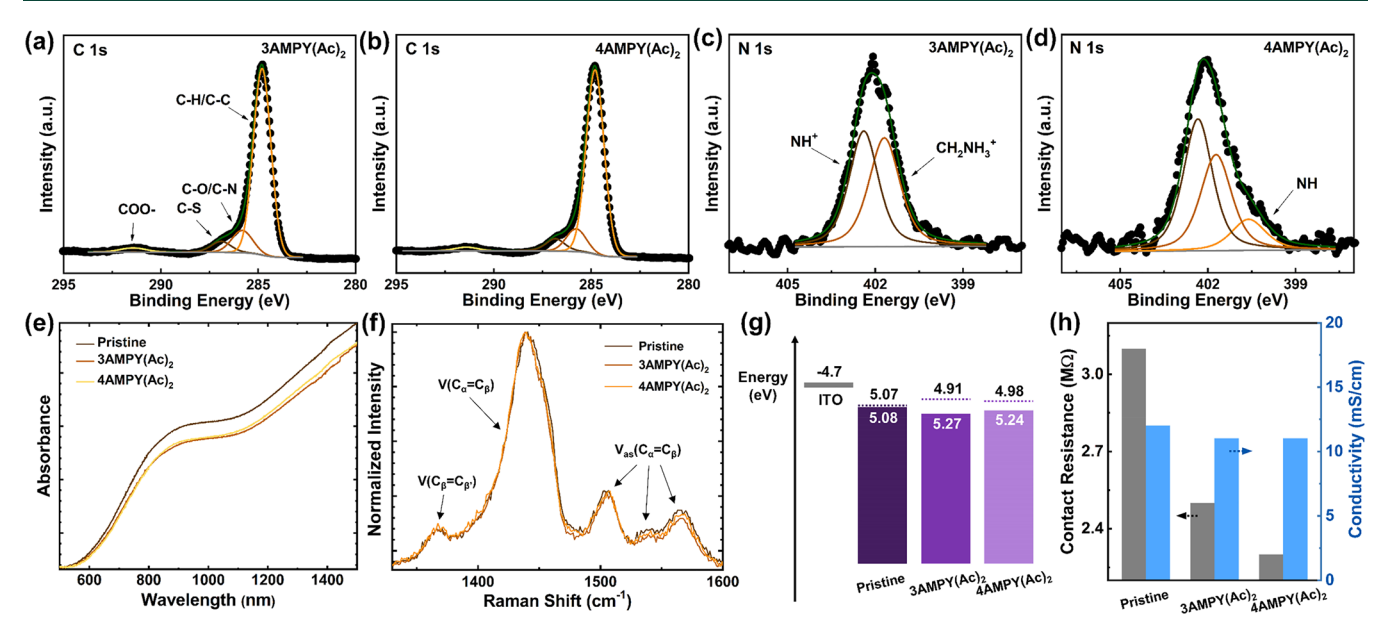


Figure 2. XPS spectra of (a, b) C 1s and (c, d) N 1s of the post-treated PEDOT:PSS with 3AMPY(Ac)<sub>2</sub> and 4AMPY(Ac)<sub>2</sub>. Comparison of (e) light absorption spectra, (f) normalized Raman spectra, (g) energy diagram, and (h) electrical properties of the post-treated PEDOT:PSS with 3AMPY(Ac)<sub>2</sub> and 4AMPY(Ac)<sub>2</sub> to those of the pristine PEDOT:PSS.

PEDOT:PSS and propose possible mechanisms as illustrated in Figure 1b,c. Even though diammonium cations are capable of tightly bridging and passivating dual-sides of PEDOT:PSS and perovskite by leveraging two active groups in a single molecule, to the best of our knowledge, their utility has not yet been identified to date among the so-far explored materials applied to PEDOT:PSS in TPSCs. <sup>28-34</sup> Aromatic diammonium cations are beneficial for the PEDOT:PSS interface passivation in several aspects. Compared with aliphatic chains, aromatic rings are hydrophobic and rigid, which are advantageous for long-term operation. The larger dielectric constants offer faster charge transfer.<sup>35</sup> Diammonium cations like 3AMPY<sup>2+</sup> and 4AMPY<sup>2+</sup> can interact with PSS<sup>-</sup> in PEDOT:PSS and halides in perovskite through the two cation groups in one molecule, as illustrated in Figure 1b,c. The interaction of 3AMPY<sup>2+</sup> and 4AMPY<sup>2</sup> with PSS<sup>-</sup> can modify the doping level of PEDOT.<sup>36</sup> The meta and para position -NH<sup>+</sup> in 3AMPY<sup>2+</sup> and 4AMPY<sup>2+</sup>, respectively, varies the degree of charge delocalization by the resonance of aromatic rings, which can affect the electrostatic interactions and hydrogen bonding of ammonium groups with the adjacent counterions and halides.<sup>35</sup> Acetate anions also have multiple impacts on both PEDOT:PSS and tin perovskites. Acetate could deprotonate PSSH to PSS- in the PEDOT:PSS top surface to reduce surface acidity while allowing tight anchoring of 3AMPY<sup>2+</sup> and 4AMPY<sup>2+</sup> via an ionic bond (Figure 1b). Acetate could retard the rapid crystallization of tin perovskite and passivate the Lewis acidic sites via the coordination with Sn<sup>2+</sup> and the occupation of halide vacancy (Figure 1c).<sup>37</sup> Holistically, our aromatic diammonium acetate salts can become an excellent choice for the modification of PEDOT:PSS and improvement of the interface and perovskite

High-resolution X-ray photoelectron spectroscopy (XPS) was utilized to examine the top  $\sim 10$  nm surface of the PEDOT:PSS. The presence of  $3AMPY(Ac)_2$  and  $4AMPY(Ac)_2$  is probed by the XPS spectra of carbon (C 1s) and nitrogen (N 1s) in Figure 2a–d. The binding energies of the

C-H/C-C, C-O/C-N, C-S, and COO peaks are 284.8, 285.8, 286.9, and 291.4 eV, respectively. Especially, the COOpeak emerges from acetate. The peaks with the binding energies of 402.3 and 401.7 eV are due to -NH+ and -CH<sub>2</sub>NH<sub>3</sub><sup>+</sup> respectively. Noticeably, 4AMPY(Ac)<sub>2</sub> emerges an additional peak of NH at a binding energy of 400.0 eV, which is likely due to the resonance structure. Figures S3a and b presented in the Supporting Information contain the XPS spectra of two sulfur (S 2p) bands corresponding to PSS and PEDOT. The dominance of PSS peaks indicates the excessive and surface-enriched PSS. 21,24 The integral ratios of PEDOT and PSS are slightly reduced to 0.11 for both PEDOT:PSS films treated with 3AMPY(Ac)<sub>2</sub> and 4AMPY(Ac)<sub>2</sub> compared to that of 0.12 for the pristine PEDOT:PSS film,<sup>48</sup> meaning a slight loss of PSS. This is further corroborated by light absorption spectra (Figure S4) where the absorption by the aromatic ring of PSS near ~220-240 nm<sup>21,24</sup> decreases slightly. On the whole, we confirm that the post-treatment slightly removes the excessive PSS while firmly anchoring 3AMPY(Ac)<sub>2</sub> and 4AMPY(Ac)<sub>2</sub> into the top surface of PEDOT:PSS. It is worthwhile to mention that the slight etching leaving residual PSS behind is beneficial for the mechanical flexibility, work function, and smooth surface. Moreover, the etching occurring in the N<sub>2</sub>-filled glovebox might reduce surface moisture for longevity.

Post-treatment-induced dedoping of PEDOT is shown by the light absorption spectra where the absorption intensities of the peaks corresponding to polaron (~900 nm) and bipolaron (~1200 nm) oxidative states of PEDOT are decreased compared to those of the pristine film. The dedoping diminishes the density of excessive hole charge carriers, boding well for interface recombination between PEDOT:PSS and perovskite. 23

Raman spectra presented in Figure 2f offer a more detailed PEDOT structural change due to dedoping. Specifically, the peaks correspond to the  $C_{\beta}=C_{\beta'}$  vibration at 1361 cm<sup>-1</sup>,  $C_{\alpha}=C_{\beta}$  symmetric stretching vibration at 1440 cm<sup>-1</sup>,  $C_{\alpha}=C_{\beta}$  asymmetric stretching vibrations at 1504 and 1570 cm<sup>-1</sup>, and

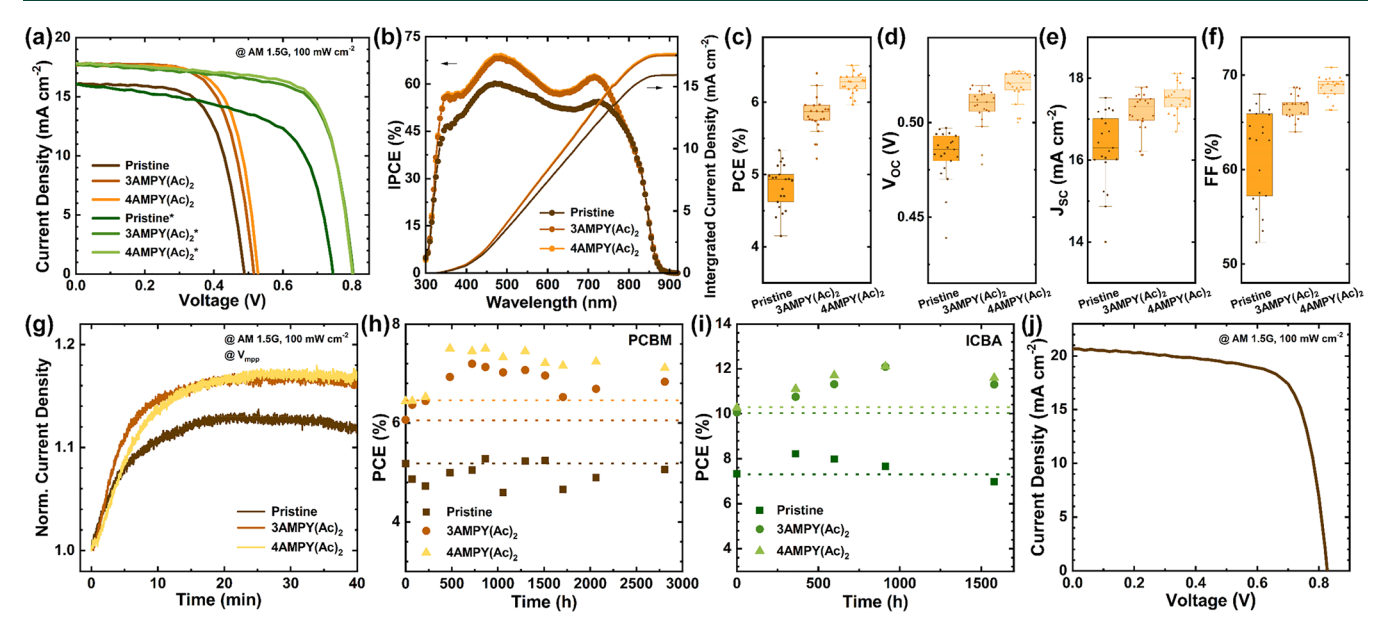


Figure 3. Photovoltaic performance of the post-treated TPSCs adopting PCBM as an ETL unless otherwise stated and measured in a glovebox. (a) Representative J-V curves where an asterisk mark means the ETL by ICBA. (b) IPCE spectra. (c-f) Statistical distribution of photovoltaic parameters. (g) MPP tracking recorded in a glovebox. (h and i) PCE evolution under dark conditions. (j) The best J-V curve extracted at the peak in panel i.

the splitting of the asymmetric vibrations at 1534 cm<sup>-1,21,24,38,39</sup> Noticeably, the symmetric vibration band becomes narrower and red-shifted for the post-treated PEDOT:PSS films, indicating the change of PEDOT conformation from benzoid to qunoid. The asymmetric vibrations at 1534 and 1570 cm<sup>-1</sup> are slightly weakened due to the dedoping. The linear-like qunoid conformation benefits charge carrier transport.

We also conducted ultraviolet photoelectron spectroscopy (UPS) measurements to study the effect of post-treatment on the electronic properties of PEDOT:PSS. The resulting UPS spectra are presented in Figure S5, and the complete energy landscape is depicted in Figure 2g. Above all, the calculated HOMO levels are well-suited for hole extraction from tin perovskites. 1,6,9,40 For the pristine PEDOT:PSS, the Fermi and highest occupied molecular orbital (HOMO) levels are very close, with an energy difference of 0.01 eV due to the high pdoping. The energy gap between the Fermi level and HOMO was calculated to be 0.36 and 0.26 eV for the PEDOT:PSS films post-treated with 3AMPY(Ac)<sub>2</sub> and 4AMPY(Ac)<sub>2</sub>, respectively. This result, in line with the light absorption, corroborates the dedoping. On the other hand, the UPS spectra allowed us to calculate WFs of 5.07 eV (pristine), 4.91 eV (3AMPY(Ac)<sub>2</sub>), and 4.98 eV (4AMPY(Ac)<sub>2</sub>). Two aspects, discussed below, need to be considered in our case. The lowered content of PSS can reduce a WF to some extent.<sup>33</sup> However, we speculate that the removal of PSS is too slight for such a noticeable WF reduction, so that it would not become a determinant. Instead, we posit that it is attributable to alteration in the local electric dipoles between PEDOT<sup>+</sup> and PSS<sup>-</sup>, which can be screened by adjacent ions. <sup>36</sup> The alteration can even be modulated with respect to increasing ion size. In our case, a small cation of H+ in PSSH is replaced with the bulky cation such as 3AMPY<sup>2+</sup> or 4AMPY<sup>2+</sup>.

Since the energy landscape altered by the dedoping can affect electrical properties, we measured conductivity and contact resistance using a transmission line method. The

results are presented in Figure 2h. Despite the dedoping, the conductivity remains nearly unaltered, 12 mS cm $^{-1}$  (pristine) to 11 mS cm $^{-1}$  (3AMPY(Ac) $_2$  and 4AMPY(Ac) $_2$ ). Importantly, the contact resistance significantly drops from 3.1 MQ (pristine) to 2.5 MQ (3AMPY(Ac) $_2$ ) and 2.3 MQ (4AMPY(Ac) $_2$ ). The counteraction of the electrically enhanced surface PEDOT:PSS by the diminished PSS and benzoid structure to dedoping can account for this. The slight variance in contact resistance between 3AMPY(Ac) $_2$  and 4AMPY(Ac) $_2$  follows the dedoping level trend. Considering Figures 1 and 2, we identify that post-treatment fosters the excellent surface states of PEDOT:PSS requiring stable and efficient hole extraction in TPSCs.

Robust tin perovskites against oxidation are pivotal to evaluating the validity of post-treatment, for which we incorporated an effective reductive additive of phenylhydrazine hydrochloride (PhCl)<sup>41</sup> into the tin perovskite (Figure S6). The perovskite composition is described in the Experimental Section in the Supporting Information. Figure S7a exhibits Xray diffraction (XRD) patterns of the final perovskites deposited onto the PEDOT:PSS. Two dominant peaks, corresponding to (100) and (200) planes, 10 appear and are alike for all samples. 10 Figure S7b shows light absorption spectra where the tin perovskites increase the absorption to a noticeable extent on the PEDOT:PSS treated with 3AMPY-(Ac)<sub>2</sub> and 4AMPY(Ac)<sub>2</sub>. Meanwhile, top-view scanning electron microscopy (SEM) images (Figure S8) show the emergence of nanoscale and shallow pinholes in the tin perovskite on the pristine PEDOT:PSS. However, the pinholes are eliminated upon post-treatment, particularly by 4AMPY-(Ac)<sub>2</sub>. We posit that post-treatment can suppress the rapid perovskite crystallization by the coordination of acetate with Sn<sup>2+</sup> toward reducing the pinholes without the expense of the crystallographic properties (Figure S7a). Taking into account that the light absorption could be weakened by the PEDOT dedoping, the slightly increased light absorption becomes more evident, and on the other hand, this can be attributed to the

ACS Energy Letters http://pubs.acs.org/journal/aelccp Letter

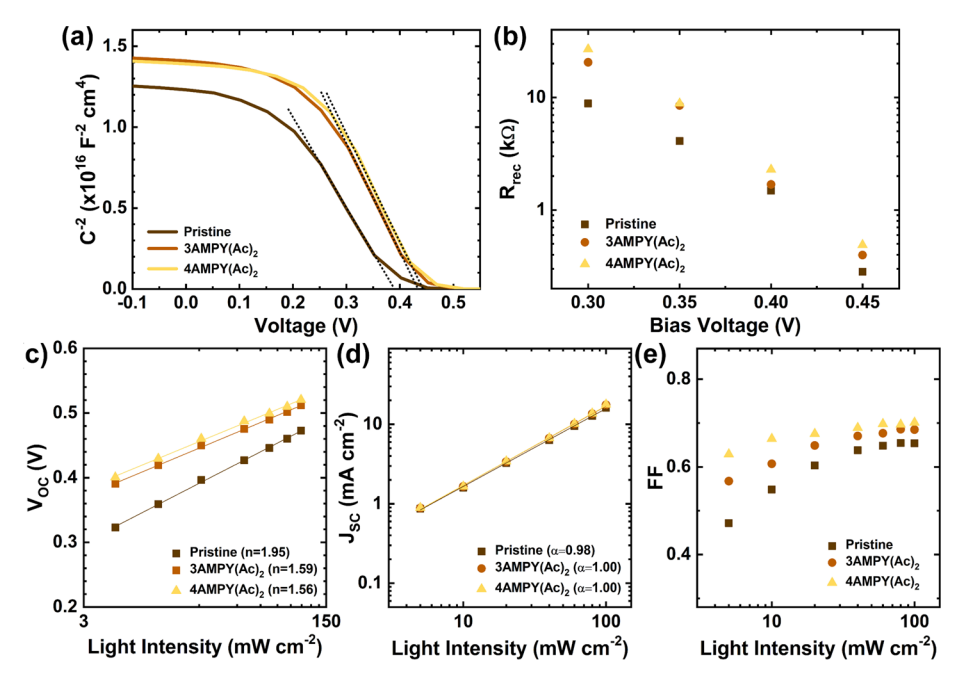


Figure 4. Plots of (a) Mott–Schottky, (b)  $R_{\rm rec}$  vs bias voltage, and plots of (c)  $V_{\rm OC}$ , (d)  $J_{\rm SC}$ , and (e) FF vs LI (0.05–1 sun), measured with the devices with the PCBM ETL.

morphological improvements. Overall, post-treatment enables the formation of tin perovskites with morphologically and optically enhanced properties.

We fabricated TPSCs possessing an inverted planar device structure of ITO/PEDOT:PSS/3AMPY(Ac)<sub>2</sub> or 4AMPY-(Ac)<sub>2</sub>/tin perovskite/PCBM/BCP/Ag as sketched in Figure 1c. Their photovoltaic performance, evaluated at standard 1 sun illumination (AM 1.5G, 100 mW cm<sup>-2</sup>), is presented in Figure 3a and Table S2. All devices show minimal hysteresis (Figure S9). 9,10,42 Overall, post-treatment did not bring an Skink in the J-V curves, which often appears by the formation of a hole extraction barrier. Instead, it steepens slopes at the open-circuit voltage  $(V_{\rm OC})$  for lower series resistances. These results corroborate that post-treatment is not hindering charge transfer but rather strengthening it owing to the lowered contact resistances. As a result, the TPSCs significantly raise a PCE from 5.2% to 6.1% by 3AMPY(Ac)<sub>2</sub> and 6.4% by 4AMPY(Ac)<sub>2</sub> driven by a concurrent rise in all photovoltaic parameters,  $V_{\rm OC}$ , short-circuit current density ( $J_{\rm SC}$ ), and fill factor (FF), listed in Table S2. Besides the charge transfer, the origin of the supreme PCE by 4AMPY(Ac)<sub>2</sub> can arise from charge recombination and is discussed in the following sections.

In order to gain generality, we replaced the ETL with ICBA. ICBA can raise  $V_{\rm OC}$  due to the higher energy level of the lowest unoccupied molecular orbital (LUMO) and suppressed iodide remote doping for an effective buildup of electrons toward increasing photovoltage. In Figure 3a, without sacrificing the photovoltaic performance trends, the ICBA boosted  $V_{\rm OC}$  from 0.526 to 0.800 V for 4AMPY(Ac)<sub>2</sub>, thereby upgrading its PCE to 10.3% (cf. 7.3% and 10.1% for pristine and 3AMPY(Ac)<sub>2</sub>, respectively). Figure 3b embraces the incident photon-to-current conversion efficiency (IPCE). Basically, the integrated photocurrent density matches well with  $J_{\rm SC}$  in the J-V curves. The IPCE increases by ~10% over the entire light wavelength region for 3AMPY(Ac)<sub>2</sub> and 4AMPY(Ac)<sub>2</sub>. IPCE is an output of coupled effects of light

absorption and charge collection. Assuming that the light absorption effect is less dominant and the separation of exciton will be instant due to the low exciton binding energy of tin perovskites, the IPCE rise can stem from superior charge collection. In Figure 3c-f, the statistical distribution of photovoltaic parameters was attained from 21 devices in which the excellent reproducibility of post-treatment is manifested by their minimal spreads, which are especially the least for 4AMPY(Ac)<sub>2</sub>.

For practical use, it is highly required to examine how posttreatment impacts device stability, for which we performed maximum power point (MPP) tracking under standard 1 sun light illumination (40 min) and dark storage measurements (~2800 h), respectively, in the absence of encapsulation. The results of MPP tracking are listed in Figure 3g. Above all, the current density rises in all devices and peaked at ~113% of the initial value for pristine devices and ~117% for 3AMPY(Ac), and 4AMPY(Ac)<sub>2</sub>. The origin of the rise can be associated with Sn(IV) in tin perovskites. The presence of Sn(IV) is nearly inevitable currently due to the easy disproportionation of Sn(II) and surrounding species, including I<sub>2</sub> and oxygen. <sup>1,41,44</sup> PhCl is reductive to Sn(IV) and also I<sub>2</sub> to stabilize not only the perovskite solution but also the perovskite film. 41,44 On the other hand, the photoreduction of another Sn(IV) healing process  $(SnI_4 + h\nu \rightarrow SnI_2 + I_2)$  can take effect. <sup>14,45</sup> Since PhCl can enter into the crystal lattice, 41 the Sn(IV) reduction by both light and PhCl occurs over the entire cross section of tin perovskite films and can be synergistic accounting for the remarkable current rise. On the other hand, the more prominent rises by the 3AMPY(Ac)<sub>2</sub> and 4AMPY(Ac)<sub>2</sub> can be a result of the effective interface passivation against the stressors such as oxygen, water, and/or ion migration. 1,41,44

Figure 3h showcases the results of dark storage measurements. In contrast to the pristine attainment of merely above 90% of the initial PCE, the 3AMPY(Ac)<sub>2</sub> and 4AMPY(Ac)<sub>2</sub> go far beyond 100% of the initial PCE on account of a concurrent rise in all photovoltaic parameters (Figure S10). At the peak,

the 3AMPY(Ac)<sub>2</sub> and 4AMPY(Ac)<sub>2</sub> increase PCE from 6.1% and 6.4% to 7.2% and 7.5%, respectively. Interestingly, the PCE rise requires longer periods of time (roughly, 500 h) in contrast to the MPP tracking results. The dark storage measurements invite the short-time exposure (<1 min) of light and bias voltage scanning for each data point to repair Sn(IV) and hence increase PCE in a relatively slower manner. Despite this, 3AMPY(Ac)<sub>2</sub> and 4AMPY(Ac)<sub>2</sub> benefit from the robust PEDOT:PSS interface, as well as the Sn(IV) repair, to firmly counteract the aforementioned stressors and to augment the PCE with time (~2800 h). On the contrary, the pristine sample is seemingly helpless with the stressors so as to cancel the Sn(IV) repair effect and to bring no progress in the PCE evolution. As ICBA takes the place of PCBM, analogous results on device aging emerged (Figures 3i and S11). In both ETLs, simultaneous increases in  $V_{\rm OC}$  and  $J_{\rm SC}$  at ~900 h are identified. However, ICBA seemingly resulted in the more prominent rises in  $J_{SC}$ , which would be attributable to its high tolerance to the stressors by the hydrophobicity<sup>46,47</sup> and suppressed iodide doping.<sup>43</sup> Most importantly, the PCE of 4AMPY(Ac)<sub>2</sub> reached an impressively high value of 12.1% after ~900 h (Figure 3j and Table S2), confirming the great potential of post-treatment for high-performance TPSCs. To the best of our knowledge, this is the best efficiency among TPSCs adopting the modified PEDOT:PSS HTLs (Table S3).

Figure 4a shows Mott-Schottky plots obtained to examine the interfacial properties of the devices in terms of built-in potential  $(V_{bi})$  and charge carrier density (N). The values of  $V_{\rm bi}$  and N were calculated from the x-axis intercept and straight negative slope (marked as a broken line), respectively (details are provided in the Supporting Information). The negative slope reflects the character of p-type semiconductors. The obtained  $V_{\rm bi}$  was 0.390, 0.429, and 0.434 V, and the N was 4.41, 3.70, and  $3.63 \times 10^{16} \text{ cm}^{-3}$  for pristine, 3AMPY(Ac)<sub>2</sub>, and 4AMPY(Ac)2, respectively. Overall, the perovskites are superior in N values to other tin perovskites<sup>42</sup> and even slightly greater than certain tin–lead perovskites. 48 The decreasing Nindicates fewer defects in the tin perovskites and hence reduced recombination, while the increasing  $V_{\rm bi}$  represents better separation and collection of charge carriers across the interfaces. In the steady-state photoluminescence (PL) spectra of Figure S12, it is revealed the reduced defects are due to the eliminated tin vacancies likely generated by Sn<sup>4+</sup> formation. Even though post-treatment shifts  $E_{\rm f}$  upward,  $V_{\rm bi}$  is rather increased toward narrowing the deficit between  $V_{\rm OC}$  and  $V_{\rm bi}$ . Larger  $V_{\rm bi}$  for the devices with the post-treated PEDOT:PSS could be attributed to the mitigation of Fermi level pinning, which is achieved by effective interface passivation by the divalent cations and acetate anions as depicted in Figure 1c. Consistently, 4AMPY(Ac)<sub>2</sub> attains the most desirable interfacial properties of  $V_{bi}$  and N owing to the best interface formation.

Impedance spectroscopy (IS) can correlate the interfacial properties with charge recombination kinetics in the devices. The raw IS spectra are presented in Figure S13, whose validity was assessed by the stable device performance after the IS measurements, as shown in Figure S14. Following the raw data fitting, the spectra of Figure 4b are produced to show the recombination resistance of  $R_{\rm rec}$  plotted as a function of the bias voltage. The  $R_{\rm rec}$  values are similar to those of the planar TPSCs and greater by approximately 10-fold than those of the mesoporous devices in spite of the varied conditions.  $^{41,42,45,50,51}$  Over the entire bias voltage range, higher

 $R_{\rm rec}$  values corresponding to suppressed interface recombination were endowed with 3AMPY(Ac)<sub>2</sub> and 4AMPY(Ac)<sub>2</sub>. Evidently, the 4AMPY(Ac)<sub>2</sub> attains the greatest  $R_{\rm rec}$  values, which are closely associated with the fewest defects and largest built-in potential together with the reduced excessive hole charge carriers by the dedoping of PEDOT.

Carrying out measurements of  $V_{\rm OC}$ ,  $J_{\rm SC}$ , and FF of devices under various light intensities (LIs) deepens insights into charge recombination kinetics. In Figure 4c showing the  $V_{\rm OC}-$ LI plots, the ideality factors (n) were obtained to be 1.95, 1.59, and 1.56 for pristine, 3AMPY(Ac)2, and 4AMPY(Ac)2, respectively. Bimolecular recombination dominates as the nvalue approaches 1, and in contrast, trap-assisted recombination dominates as the n value is closer to 2.52 The principal reason for the n value being between 1 and 2 is that the trap density of the tin perovskites (> $10^{16}$  cm<sup>-3</sup>) exceeds the photogenerated charge density ( $\leq 10^{15}$  cm<sup>-3</sup>). Nonetheless, post-treatment takes effect toward suppressing trap-assisted recombination markedly. Figure 4d exhibits the  $J_{SC}$ -LI plots, whose slopes enable the calculation of scaling exponent  $(\alpha)$ values. While an  $\alpha$  value close to 1 is desirable, the obtained  $\alpha$ values are 0.98 for pristine and 1.00 for 3AMPY(Ac)2 and 4AMPY(Ac)<sub>2</sub>. We note that all of the  $\alpha$  values are in a similar range, indicating the space-charge effect is negligible.<sup>53</sup> Figure 4e contains FF-LI plots where FF rises by ~0.18, ~0.11, and ~0.07 for pristine, 3AMPY(Ac)<sub>2</sub>, and 4AMPY(Ac)<sub>2</sub>, respectively. This FF evolution is distinct from that of lead PSCs. 52 We posit that the abundant background current that is independent of light intensity becomes pronounced at low light intensities, accounting for such FF evolution. Nevertheless, it is important to remark that post-treatment is effective to avoid FF evolution in particular with the 4AMPY(Ac)<sub>2</sub>. By the above analysis on the charge kinetics, we now confirm that the suppressed interface recombination, evident with the IS spectra, originates from the reduced trapassisted recombination thanks to the ameliorated interface of PEDOT:PSS and tin perovskite by post-treatment.

In this research, we explicitly show how to customize the commercial product of PEDOT:PSS via ameliorating its surface with aromatic diammonium acetate salts while preserving the essential properties in bulk toward amplifying hole extraction characteristics for tin perovskite solar cells with high efficiency and longevity. The materials and methodologies of our development can be extended to other perovskite- and PEDOT:PSS-based bio, energy, and electronic applications. Moreover, they can expand on surface and interface engineering to gain broader scope, thereby laying a critical bridging stone on paths to diverse applications.

### ASSOCIATED CONTENT

### Supporting Information

The Supporting Information is available free of charge at https://pubs.acs.org/doi/10.1021/acsenergylett.3c00583.

Experimental section, current-voltage characteristics, AFM, PL, XRD, XPS, UPS, SEM, light absorption spectra, and EIS (PDF)

# AUTHOR INFORMATION

# **Corresponding Author**

Qiuming Yu — Robert Frederick Smith School of Chemical and Biomolecular Engineering, Cornell University, Ithaca, New York 14853, United States; orcid.org/0000-0002-2401-4664; Email: qy10@cornell.edu

### **Authors**

- Donghoon Song Robert Frederick Smith School of Chemical and Biomolecular Engineering, Cornell University, Ithaca, New York 14853, United States; orcid.org/0000-0003-0914-1507
- Hao Li Robert Frederick Smith School of Chemical and Biomolecular Engineering, Cornell University, Ithaca, New York 14853, United States; orcid.org/0000-0002-9433-1198
- Yuanze Xu Robert Frederick Smith School of Chemical and Biomolecular Engineering, Cornell University, Ithaca, New York 14853, United States; © orcid.org/0000-0002-4873-6629

Complete contact information is available at: https://pubs.acs.org/10.1021/acsenergylett.3c00583

## **Author Contributions**

The manuscript was written through contributions of all authors. All authors have given approval to the final version of the manuscript.

### **Notes**

The authors declare no competing financial interest.

# ACKNOWLEDGMENTS

We acknowledge the financial support from the National Science Foundation (NSF) (ECCS-2054942 and EPM-2114350). This work made use of the Cornell Center for Materials Research Shared Facilities, which are supported through the NSF MRSEC program (DMR-1719875). We thank Grace Gentner for AFM imaging.

### REFERENCES

- (1) Pitaro, M.; Tekelenburg, E. K.; Shao, S.; Loi, M. A. Tin Halide Perovskites: From Fundamental Properties to Solar Cells. *Adv. Mater.* **2022**, *34* (1), 2105844.
- (2) Cao, J.; Yan, F. Recent Progress in Tin-Based Perovskite Solar Cells. *Energy Environ. Sci.* **2021**, *14* (3), 1286–1325.
- (3) Wu, T.; Liu, X.; Luo, X.; Lin, X.; Cui, D.; Wang, Y.; Segawa, H.; Zhang, Y.; Han, L. Lead-Free Tin Perovskite Solar Cells. *Joule* **2021**, *5* (4), 863–886.
- (4) Diau, E. W.-G.; Jokar, E.; Rameez, M. Strategies To Improve Performance and Stability for Tin-Based Perovskite Solar Cells. *ACS Energy Lett.* **2019**, *4* (8), 1930–1937.
- (5) Ke, W.; Stoumpos, C. C.; Kanatzidis, M. G. Unleaded" Perovskites: Status Quo and Future Prospects of Tin-Based Perovskite Solar Cells. *Adv. Mater.* **2019**, *31* (47), 1803230.
- (6) Jiang, X.; Zang, Z.; Zhou, Y.; Li, H.; Wei, Q.; Ning, Z. Tin Halide Perovskite Solar Cells: An Emerging Thin-Film Photovoltaic Technology. *Acc. Mater. Res.* **2021**, *2* (4), 210–219.
- (7) Cao, H.; Zhang, Z.; Zhang, M.; Gu, A.; Yu, H.; Ban, H.; Sun, Q.; Shen, Y.; Zhang, X.-L.; Zhu, J.; Wang, M. The Effect of Defects in Tin-Based Perovskites and Their Photovoltaic Devices. *Mater. Today Phys.* **2021**, *21*, 100513.
- (8) Rühle, S. Tabulated Values of the Shockley-Queisser Limit for Single Junction Solar Cells. *Sol. Energy* **2016**, *130*, 139–147.
- (9) Yu, B.-B.; Chen, Z.; Zhu, Y.; Wang, Y.; Han, B.; Chen, G.; Zhang, X.; Du, Z.; He, Z. Heterogeneous 2D/3D Tin-Halides Perovskite Solar Cells with Certified Conversion Efficiency Breaking 14%. Adv. Mater. 2021, 33 (36), 2102055.
- (10) Jiang, X.; Li, H.; Zhou, Q.; Wei, Q.; Wei, M.; Jiang, L.; Wang, Z.; Peng, Z.; Wang, F.; Zang, Z.; Xu, K.; Hou, Y.; Teale, S.; Zhou, W.; Si, R.; Gao, X.; Sargent, E. H.; Ning, Z. One-Step Synthesis of SnI2-

- (DMSO)x Adducts for High-Performance Tin Perovskite Solar Cells. J. Am. Chem. Soc. 2021, 143 (29), 10970–10976.
- (11) Park, J.; Kim, J.; Yun, H.-S.; Paik, M. J.; Noh, E.; Mun, H. J.; Kim, M. G.; Shin, T. J.; Seok, S., Il. Controlled Growth of Perovskite Layers with Volatile Alkylammonium Chlorides. *Nature* **2023**, *616*, 724–730.
- (12) Kumar, M. H.; Dharani, S.; Leong, W. L.; Boix, P. P.; Prabhakar, R. R.; Baikie, T.; Shi, C.; Ding, H.; Ramesh, R.; Asta, M.; Graetzel, M.; Mhaisalkar, S. G.; Mathews, N. Lead-Free Halide Perovskite Solar Cells with High Photocurrents Realized through Vacancy Modulation. *Adv. Mater.* **2014**, *26* (41), 7122–7127.
- (13) Lee, S. J.; Shin, S. S.; Kim, Y. C.; Kim, D.; Ahn, T. K.; Noh, J. H.; Seo, J.; Seok, S., Il. Fabrication of Efficient Formamidinium Tin Iodide Perovskite Solar Cells through SnF2-Pyrazine Complex. J. Am. Chem. Soc. 2016, 138 (12), 3974-3977.
- (14) Sanchez-Diaz, J.; Sánchez, R. S.; Masi, S.; Kreĉmarová, M.; Alvarez, A. O.; Barea, E. M.; Rodriguez-Romero, J.; Chirvony, V. S.; Sánchez-Royo, J. F.; Martinez-Pastor, J. P.; Mora-Seró, I. Tin Perovskite Solar Cells with > 1,300 h of Operational Stability in N2 through a Synergistic Chemical Engineering Approach. *Joule* 2022, 6 (4), 861–883.
- (15) Shao, S.; Liu, J.; Portale, G.; Fang, H. H.; Blake, G. R.; ten Brink, G. H.; Koster, L. J. A.; Loi, M. A. Highly Reproducible Sn-Based Hybrid Perovskite Solar Cells with 9% Efficiency. *Adv. Energy Mater.* **2018**, 8 (4), 1702019.
- (16) Zhou, J.; Hao, M.; Zhang, Y.; Ma, X.; Dong, J.; Lu, F.; Wang, J.; Wang, N.; Zhou, Y. Chemo-Thermal Surface Dedoping for High-Performance Tin Perovskite Solar Cells. *Matter* **2022**, *5* (2), 683–693.
- (17) Kamarudin, M. A.; Sahamir, S. R.; Nishimura, K.; Iikubo, S.; Yoshino, K.; Minemoto, T.; Shen, Q.; Hayase, S. Suppression of Defect and Trap Density through Dimethylammonium-Substituted Tin Perovskite Solar Cells. ACS Mater. Lett. 2022, 4 (9), 1855–1862.
- (18) Wang, S.; Wu, C.; Xie, L.; Ding, L.; Hao, F. Pseudohalide-Modulated Crystallization for Efficient Quasi-2D Tin Perovskite Solar Cells with Minimized Voltage Deficit. ACS Mater. Lett. **2023**, *5*, 936–943
- (19) Qiu, J.; Xia, Y.; Zheng, Y.; Hui, W.; Gu, H.; Yuan, W.; Yu, H.; Chao, L.; Niu, T.; Yang, Y.; Gao, X.; Chen, Y.; Huang, W. 2D Intermediate Suppression for Efficient Ruddlesden—Popper (RP) Phase Lead-Free Perovskite Solar Cells. ACS Energy Lett. 2019, 4 (7), 1513—1520.
- (20) Liao, W.; Zhao, D.; Yu, Y.; Grice, C. R.; Wang, C.; Cimaroli, A. J.; Schulz, P.; Meng, W.; Zhu, K.; Xiong, R.-G.; Yan, Y. Lead-Free Inverted Planar Formamidinium Tin Triiodide Perovskite Solar Cells Achieving Power Conversion Efficiencies up to 6.22%. *Adv. Mater.* **2016**, 28 (42), 9333–9340.
- (21) Fan, X.; Nie, W.; Tsai, H.; Wang, N.; Huang, H.; Cheng, Y.; Wen, R.; Ma, L.; Yan, F.; Xia, Y. PEDOT:PSS for Flexible and Stretchable Electronics: Modifications, Strategies, and Applications. *Adv. Sci.* **2019**, *6* (19), 1900813.
- (22) Abdel-Shakour, M.; Chowdhury, T. H.; Matsuishi, K.; Bedja, I.; Moritomo, Y.; Islam, A. High-Efficiency Tin Halide Perovskite Solar Cells: The Chemistry of Tin (II) Compounds and Their Interaction with Lewis Base Additives during Perovskite Film Formation. *Sol. RRL* 2021, 5 (1), 2000606.
- (23) Park, K.; Lee, J.-H.; Lee, J.-W. Surface Defect Engineering of Metal Halide Perovskites for Photovoltaic Applications. *ACS Energy Lett.* **2022**, *7* (3), 1230–1239.
- (24) Niu, Z.; Zheng, E.; Dong, H.; Tosado, G. A.; Yu, Q. Manipulation of PEDOT:PSS with Polar and Nonpolar Solvent Post-Treatment for Efficient Inverted Perovskite Solar Cells. ACS Appl. Energy Mater. 2020, 3 (10), 9656–9666.
- (25) Zhou, J.; Anjum, D. H.; Chen, L.; Xu, X.; Ventura, I. A.; Jiang, L.; Lubineau, G. The Temperature-Dependent Microstructure of PEDOT/PSS Films: Insights from Morphological, Mechanical and Electrical Analyses. *J. Mater. Chem. C* **2014**, 2 (46), 9903–9910.
- (26) Ni, Z.; Bao, C.; Liu, Y.; Jiang, Q.; Wu, W.-Q.; Chen, S.; Dai, X.; Chen, B.; Hartweg, B.; Yu, Z.; Holman, Z.; Huang, J. Resolving

- Spatial and Energetic Distributions of Trap States in Metal Halide Perovskite Solar Cells. *Science* **2020**, *367* (6484), 1352–1358.
- (27) Ramos-Villaseñor, J. M.; Rodríguez-Cárdenas, E.; Barrera Díaz, C. E.; Frontana-Uribe, B. A. Review—Use of 1,1,1,3,3,3—Hexafluoro—2—Propanol (HFIP) Co-Solvent Mixtures in Organic Electrosynthesis. *J. Electrochem. Soc.* **2020**, *167* (15), 155509.
- (28) Yang, W.-F.; Cao, J.-J.; Chen, J.; Wang, K.-L.; Dong, C.; Wang, Z.-K.; Liao, L.-S. Nicotinamide-Modified PEDOT:PSS for High Performance Indoor and Outdoor Tin Perovskite Photovoltaics. *Sol. RRL* 2021, 5 (12), 2100713.
- (29) Shih, C.-C.; Wu, C.-G. Synergistic Engineering of the Conductivity and Surface Properties of PEDOT:PSS-Based HTLs for Inverted Tin Perovskite Solar Cells to Achieve Efficiency over 10%. ACS Appl. Mater. Interfaces 2022, 14 (14), 16125–16135.
- (30) Liu, X.; Wang, Y.; Xie, F.; Yang, X.; Han, L. Improving the Performance of Inverted Formamidinium Tin Iodide Perovskite Solar Cells by Reducing the Energy-Level Mismatch. *ACS Energy Lett.* **2018**, 3 (5), 1116–1121.
- (31) Chen, J.; Zhao, X.; Cheng, Y.; Qian, J.; Wang, M.; Shen, W.; Cao, K.; Huang, Y.; Hui, W.; Gu, Y.; Chen, Y.; Gao, X.; Chen, S. Hydroxyl-Rich d-Sorbitol to Address Transport Layer/Perovskite Interfacial Issues toward Highly Efficient and Stable 2D/3D Tin-Based Perovskite Solar Cells. *Adv. Opt. Mater.* **2021**, *9* (22), 2100755.
- (32) Ran, C.; Xi, J.; Gao, W.; Yuan, F.; Lei, T.; Jiao, B.; Hou, X.; Wu, Z. Bilateral Interface Engineering toward Efficient 2D–3D Bulk Heterojunction Tin Halide Lead-Free Perovskite Solar Cells. *ACS Energy Lett.* **2018**, 3 (3), 713–721.
- (33) Chen, Y.; Cao, K.; Cheng, Y.; Shen, H.; Du, C.; Wang, Q.; Chen, C.; Cui, H.; Lan, T.; Liu, L.; Shen, W.; Chen, S. P-Type Dopants As Dual Function Interfacial Layer for Efficient and Stable Tin Perovskite Solar Cells. *Sol. RRL* **2021**, *5* (5), 2100068.
- (34) Chen, M.; Kapil, G.; Wang, L.; Razey Sahamir, S.; Baranwal, A. K.; Nishimura, K.; Sanehira, Y.; Zhang, Z.; Akmal Kamarudin, M.; Shen, Q.; Hayase, S. High Performance Wide Bandgap Lead-Free Perovskite Solar Cells by Monolayer Engineering. *Chem. Eng. J.* **2022**, 436, 135196.
- (35) Li, X.; Ke, W.; Traoré, B.; Guo, P.; Hadar, I.; Kepenekian, M.; Even, J.; Katan, C.; Stoumpos, C. C.; Schaller, R. D.; Kanatzidis, M. G. Two-Dimensional Dion–Jacobson Hybrid Lead Iodide Perovskites with Aromatic Diammonium Cations. *J. Am. Chem. Soc.* **2019**, *141* (32), 12880–12890.
- (36) Liu, T.; Sun, L.; Dong, X.; Jiang, Y.; Wang, W.; Xie, C.; Zeng, W.; Liu, Y.; Qin, F.; Hu, L.; Zhou, Y. Low-Work-Function PEDOT Formula as a Stable Interlayer and Cathode for Organic Solar Cells. *Adv. Funct. Mater.* **2021**, *31* (51), 2107250.
- (37) Li, G.; Su, Z.; Li, M.; Yang, F.; Aldamasy, M. H.; Pascual, J.; Yang, F.; Liu, H.; Zuo, W.; Di Girolamo, D.; Iqbal, Z.; Nasti, G.; Dallmann, A.; Gao, X.; Wang, Z.; Saliba, M.; Abate, A. Ionic Liquid Stabilizing High-Efficiency Tin Halide Perovskite Solar Cells. *Adv. Energy Mater.* **2021**, *11* (32), 2101539.
- (38) Tosado, G. A.; Zheng, E.; Yu, Q. Tuning Cesium—Guanidinium in Formamidinium Tin Triiodide Perovskites with an Ethylenediammonium Additive for Efficient and Stable Lead-Free Perovskite Solar Cells. *Mater. Adv.* **2020**, *1* (9), 3507–3517.
- (39) Zheng, E.; Jain, P.; Dong, H.; Niu, Z.; Chen, S.; Zhong, S.; Yu, Q. Chemical Polymerization of Hydroxymethyl and Chloromethyl Functionalized PEDOT:PSS. ACS Appl. Polym. Mater. 2019, 1 (11), 3103–3114.
- (40) Dong, H.; Zheng, E.; Niu, Z.; Zhang, X.; Lin, Y.-Y.; Jain, P.; Yu, Q. Hydroxymethyl-Functionalized PEDOT-MeOH:PSS for Perovskite Solar Cells. *ACS Appl. Mater. Interfaces* **2020**, *12* (15), 17571–17582.
- (41) Wang, C.; Gu, F.; Zhao, Z.; Rao, H.; Qiu, Y.; Cai, Z.; Zhan, G.; Li, X.; Sun, B.; Yu, X.; Zhao, B.; Liu, Z.; Bian, Z.; Huang, C. Self-Repairing Tin-Based Perovskite Solar Cells with a Breakthrough Efficiency Over 11%. *Adv. Mater.* **2020**, 32 (31), 1907623.
- (42) Jokar, E.; Chien, C.-H.; Fathi, A.; Rameez, M.; Chang, Y.-H.; Diau, E. W.-G. Slow Surface Passivation and Crystal Relaxation with Additives to Improve Device Performance and Durability for Tin-

- Based Perovskite Solar Cells. Energy Environ. Sci. 2018, 11 (9), 2353–2362.
- (43) Jiang, X.; Wang, F.; Wei, Q.; Li, H.; Shang, Y.; Zhou, W.; Wang, C.; Cheng, P.; Chen, Q.; Chen, L.; Ning, Z. Ultra-High Open-Circuit Voltage of Tin Perovskite Solar Cells via an Electron Transporting Layer Design. *Nat. Commun.* **2020**, *11* (1), 1245.
- (44) Chen, S.; Xiao, X.; Gu, H.; Huang, J. Iodine Reduction for Reproducible and High-Performance Perovskite Solar Cells and Modules. *Sci. Adv.* **2021**, *7* (10), eabe8130.
- (45) Song, D.; Narra, S.; Li, M.-Y.; Lin, J.-S.; Diau, E. W.-G. Interfacial Engineering with a Hole-Selective Self-Assembled Monolayer for Tin Perovskite Solar Cells via a Two-Step Fabrication. *ACS Energy Lett.* **2021**, *6* (12), 4179–4186.
- (46) Sun, Q.; Zhang, F.; Wang, J.; An, Q.; Zhao, C.; Li, L.; Teng, F.; Hu, B. A Two-Step Strategy to Clarify the Roles of a Solution Processed PFN Interfacial Layer in Highly Efficient Polymer Solar Cells. J. Mater. Chem. A 2015, 3 (36), 18432–18441.
- (47) Tsai, C.-L.; Lu, Y.-C.; Chiang, S.-E.; Yu, C.-M.; Cheng, H.-M.; Hsu, C.-L.; Chiu, K. Y.; Chang, S. H. Bright and Fast-Response Perovskite Light-Emitting Diodes with an ICBA:Modified-C60 Nanocomposite Electrical Confinement Layer. *Nanoscale* **2020**, *12* (6), 4061–4068.
- (48) Lin, R.; Xiao, K.; Qin, Z.; Han, Q.; Zhang, C.; Wei, M.; Saidaminov, M. I.; Gao, Y.; Xu, J.; Xiao, M.; Li, A.; Zhu, J.; Sargent, E. H.; Tan, H. Monolithic All-Perovskite Tandem Solar Cells with 24.8% Efficiency Exploiting Comproportionation to Suppress Sn(Ii) Oxidation in Precursor Ink. *Nat. Energy* 2019, 4 (10), 864–873.
- (49) Guerrero, A.; Marchesi, L. F.; Boix, P. P.; Ruiz-Raga, S.; Ripolles-Sanchis, T.; Garcia-Belmonte, G.; Bisquert, J. How the Charge-Neutrality Level of Interface States Controls Energy Level Alignment in Cathode Contacts of Organic Bulk-Heterojunction Solar Cells. *ACS Nano* **2012**, *6* (4), 3453–3460.
- (50) Tsai, C. M.; Mohanta, N.; Wang, C. Y.; Lin, Y. P.; Yang, Y. W.; Wang, C. L.; Hung, C. H.; Diau, E. W. G. Formation of Stable Tin Perovskites Co-Crystallized with Three Halides for Carbon-Based Mesoscopic Lead-Free Perovskite Solar Cells. *Angew. Chem., Int. Ed.* **2017**, *56* (44), 13819–13823.
- (51) Song, D.; Hsu, L. Y.; Tseng, C.-M.; Diau, E. W.-G. Solution-Processed ITO Nanoparticles as Hole-Selective Electrodes for Mesoscopic Lead-Free Perovskite Solar Cells. *Mater. Adv.* **2021**, 2 (2), 754–759.
- (52) Glowienka, D.; Galagan, Y. Light Intensity Analysis of Photovoltaic Parameters for Perovskite Solar Cells. *Adv. Mater.* **2022**, 34 (2), 2105920.
- (53) Wilken, S.; Sandberg, O. J.; Scheunemann, D.; Österbacka, R. Watching Space Charge Build Up in an Organic Solar Cell. *Sol. RRL* **2020**, *4* (3), 1900505.